

# Time-Asymmetric Protocol Optimization for Efficient Free Energy Estimation

Adrienne Zhong\* and Benjamin Kuznets-Speck\*

Department of Physics, University of California, Berkeley, CA, 94720, USA and  
Biophysics Graduate Group, University of California, Berkeley, CA, 94720, USA

Michael R. DeWeese

Department of Physics, University of California, Berkeley, CA, 94720 and  
Redwood Center For Theoretical Neuroscience and Helen Wills Neuroscience Institute,  
University of California, Berkeley, Berkeley, CA, 94720

(Dated: April 2023)

The free-energy difference  $\Delta F$  between two high-dimensional systems is an important yet computationally difficult quantity to compute. We demonstrate that the microscopic fluctuation theorem for an unconventional definition of work introduced by Vaikuntanathan and Jarzynski (2008) connects path ensembles that are driven by protocols unequal under time-reversal, allowing us to use a low-variance Bennett acceptance ratio  $\Delta F$  estimator on bi-directional measurements from time-asymmetric processes. It has been shown before that counterdiabatic protocols give zero-variance work measurements for this definition. Motivated by this, we propose an on-the-fly adaptive importance sampling policy optimization algorithm that iteratively improves the efficiency of the time-asymmetric protocols. This algorithm requires minimal computational overhead, and uses all the samples collected in previous iterations to (1) update the protocol, and (2) provide a  $\Delta F$  estimate. We test our algorithm on three models of varying complexity, finding that with just  $10^3$  bi-directional work samples our algorithm yields  $\Delta F$  estimates that are  $\sim 10^2 - 10^4$  times lower in mean squared error than the linear interpolation protocol with which it was initialized.

Free energy differences  $\Delta F = F_B - F_A$  between pairs of potential energy functions  $U_A(\mathbf{x})$  and  $U_B(\mathbf{x})$  are sought after by physicists, chemists, and pharmaceutical scientists alike [1–6]. Here,  $\mathbf{x} \in \mathbb{R}^d$  is the configuration space coordinate, and the free energy for each potential is defined as  $F_{A,B} = -\beta^{-1} \ln \int e^{-\beta U_{A,B}(\mathbf{x}')} d\mathbf{x}'$ , where  $\beta = (k_B T)^{-1}$  is inverse temperature. For high dimensional systems,  $\Delta F$  can only be calculated numerically through sampling methods, which can be computationally costly and slow to converge [4]. Here we develop an adaptive method to learn efficient finite-time protocols that approximate a counterdiabatic force that estimates  $\Delta F$  with zero variance.

One class of estimators take work measurements as input from protocols  $U(\mathbf{x}, t)$  that “switch”  $U(\mathbf{x}, 0) = U_A(\mathbf{x}) \rightarrow U(\mathbf{x}, t_f) = U_B(\mathbf{x})$  in finite time  $t_f$ . Because the work, traditionally defined for each trajectory  $\mathbf{x}(t)|_{t \in [0, t_f]}$  as

$$W_{\text{trad}}[\mathbf{x}(t)] = \int_0^{t_f} \frac{\partial U}{\partial t}(\mathbf{x}(t), t) dt \quad (1)$$

satisfies the Jarzynski equality

$$\langle e^{-\beta W} \rangle = e^{-\beta \Delta F}, \quad (2)$$

the Jarzynski estimator  $\widehat{\Delta F}_{\text{Jar}} = -\beta^{-1} \ln (n_s^{-1} \sum_{i=1}^{n_s} e^{-\beta W_{\text{trad}}^i})$  may be applied to work measurements  $\{W_{\text{trad}}^i | i = 1, \dots, n_s\}$ . Unfortunately this estimator can be slow to converge, because the average is often dominated by rare events.

Estimators that use bi-directional work measurements (i.e., those that also consider  $U_B \rightarrow U_A$  switching processes) generally have lower variance than uni-directional

work estimators [7]. In particular, Shirts et al. in [8] showed that if forward  $\{W_F^i | i = 1, \dots, n_s\}$  and reverse work measurements  $\{W_R^i | i = 1, \dots, n_s\}$ , assumed here to be equal in number for simplicity, are collected from forward and reverse protocols satisfying Crook’s Fluctuation Theorem

$$P_F(+W) = P_R(-W) e^{\beta(W - \Delta F)}, \quad (3)$$

then the Bennett acceptance ratio estimator  $\widehat{\Delta F}_{\text{BAR}}$  [9], defined implicitly as the  $\Delta F$  satisfying

$$\sum_{i=1}^{n_s} \frac{1}{1 + e^{-\beta(W_F^i - \Delta F)}} - \sum_{j=1}^{n_s} \frac{1}{1 + e^{-\beta(W_R^j + \Delta F)}} = 0, \quad (4)$$

is the lowest-variance asymptotically-unbiased estimator. Bi-directional measurements of  $W_{\text{trad}}$  for a pair of time-reversal-symmetric forward and reverse protocols satisfy Eq. (3) [10, 11], but measurements can also be collected from *mixtures* of different measurement-protocol pairs

$$P_F(\cdot) = \sum_i \alpha_i P_F^i(\cdot) \quad \text{and} \quad P_R(\cdot) = \sum_i \alpha_i P_R^i(\cdot) \quad (5)$$

with  $\sum_i \alpha_i = 1$ , as long as each  $(P_F^i, P_R^i)$  pair satisfies Eq. (3).

In this Letter, we consider the non-standard definition of work introduced in [12], for which there exists finite-time counterdiabatic driving protocols that give zero-variance work measurements. We explicitly show it satisfies the fluctuation theorem Eq. (3) for measurements that are produced from forward and reverse protocols that are *unequal* under time-reversal. We

propose an algorithm that iteratively improves time-asymmetric protocols from bi-directional measurements collected from all previous iterations. Finally, for three examples of increasing complexity, we demonstrate that  $10^3$  bi-directional measurements made under our protocol optimization algorithm give  $\Delta F$  estimates that are a factor of  $\sim 10^2 - 10^4$  lower in mean squared error than  $10^3$  bi-directional measurements made with the naive linear interpolation protocol with which it was initialized.

*Time-asymmetric work.*—For our setting we consider a time-varying potential energy  $U_0(\mathbf{x}, t)$  for  $t \in [0, t_f]$ , that begins at  $U_0(x, 0) = U_A(\mathbf{x})$  and ends at  $U_0(\mathbf{x}, t_f) = U_B(\mathbf{x})$ . To this we add an additional potential  $U_1(\mathbf{x}, t)$  that satisfies  $U_1(\mathbf{x}, 0) = U_1(\mathbf{x}, t_f) = 0$ . In the overdamped limit,  $\mathbf{x}(t)$  evolves under the Langevin equation

$$\dot{\mathbf{x}} = -\nabla(U_0 + U_1) + \boldsymbol{\eta}(t) \quad \text{with} \quad \mathbf{x}(0) \sim \rho_A(\cdot). \quad (6)$$

Here,  $\rho_A(\mathbf{x}) = e^{-\beta[U_A(\mathbf{x}) - F_A]}$  is the equilibrium distribution for  $U_A(\mathbf{x})$ , and  $\boldsymbol{\eta}(t)$  is  $d$ -dimensional Gaussian white noise specified by  $\langle \eta_i(t) \rangle = 0$  and  $\langle \eta_i(t) \eta_j(t') \rangle = 2\beta^{-1} \delta_{ij} \delta(t - t')$  [13].

In [12] the authors introduced the non-conventional work definition, which in our setting is

$$W[\mathbf{x}(t)] = \int_0^{t_f} \frac{\partial U_0}{\partial t} - \nabla U_0 \cdot \nabla U_1 + \beta^{-1} \nabla^2 U_1 dt \quad (7)$$

( $\nabla^2$  is the scalar Laplace operator), and demonstrated that, remarkably,  $W[\mathbf{x}(t)] = \Delta F$  for *every* trajectory  $\mathbf{x}(t)$ , if  $U_1(\mathbf{x}, t)$  gives the counterdiabatic force for  $U_0(\mathbf{x}, t)$ , meaning

$$\frac{\partial \rho_0}{\partial t} = \nabla \cdot (\rho_0 \nabla U_1) \quad \text{for} \quad \rho_0(\mathbf{x}, t) := e^{-\beta[U_0(\mathbf{x}, t) - F_0(t)]}. \quad (8)$$

Here  $\rho_0(\mathbf{x}, t)$  is the instantaneous equilibrium distribution corresponding to  $U_0(\mathbf{x}, t)$ , with time-dependent free energy  $F_0(t) = -\beta^{-1} \ln \int e^{-\beta U_0(\mathbf{x}', t)} d\mathbf{x}'$  satisfying  $F_0(0) = F_A$  and  $F_0(t_f) = F_B$  [14–16]. Under these conditions, the time-dependent probability distribution for Eq. (6) is always in instantaneous equilibrium with  $U_0(\mathbf{x}, t)$ .

Indeed, expanding Eq. (8) yields

$$\frac{\partial U_0}{\partial t} - \nabla U_0 \cdot \nabla U_1 + \beta^{-1} \nabla^2 U_1 = \frac{dF_0}{dt}, \quad (9)$$

which, when plugged into Eq. (7), shows that the time-asymmetric work  $W[\mathbf{x}(t)] = \int_0^{t_f} \dot{F}_0(t) dt = F_0(t_f) - F_0(0) = \Delta F$  for *every* trajectory  $\mathbf{x}(t)$ . With optimally chosen  $U_0(\mathbf{x}, t)$  and  $U_1(\mathbf{x}, t)$ , the free energy difference may be obtained from simulating a single finite-time trajectory. Unfortunately, Eq. (9) is typically infeasible to solve for multidimensional systems, and to formulate the PDE,  $\dot{F}_0(t)$ , and therefore  $\Delta F$ , must already be known.

*Microscopic fluctuation theorem*—In the late 1990s, Crooks [10, 11] discovered that the traditional work

(Eq. (1)) satisfies the microscopic fluctuation theorem

$$W[\mathbf{x}(t)] = \Delta F + \beta^{-1} \ln \frac{P[\mathbf{x}(t)]}{\tilde{P}[\tilde{\mathbf{x}}(t)]}, \quad (10)$$

where  $P[\mathbf{x}(t)]$  is the probability of observing a trajectory  $\mathbf{x}(t)$ , and  $\tilde{P}[\tilde{\mathbf{x}}(t)]$  is the probability of observing its time-reversed trajectory  $\tilde{\mathbf{x}}(t) = \mathbf{x}(t_f - t)$  in a “reverse” path ensemble driven by the protocol  $\tilde{U}(\mathbf{x}, t) = U(\mathbf{x}, t_f - t)$ . In order to gain insight into the non-conventional work definition Eq. (7), we examine its associated microscopic fluctuation theorem.

In our overdamped setting, the probability of realizing a trajectory  $\mathbf{x}(t)$  from the dynamics Eq. (6) may be formally expressed, up to a normalization factor, as

$$P[\mathbf{x}(t)] = \rho_A(\mathbf{x}(0)) e^{-\beta S[\mathbf{x}(t)]}, \quad (11)$$

where

$$S[\mathbf{x}(t)] = (\text{I}) \int_0^{t_f} \frac{|\dot{\mathbf{x}} + \nabla(U_0 + U_1)|^2}{4} dt, \quad (12)$$

is the Onsager-Machlup action functional [17]. We use (I) to indicate that the integral is taken in an Itô sense [18]. After Eqs. (7) and (11) are plugged into Eq. (10), straightforward manipulations under the rules of stochastic calculus [18] yield

$$\begin{aligned} \tilde{P}[\tilde{\mathbf{x}}(t)] &= e^{-\beta\{U_A(\mathbf{x}(0)) - F_A + S[\mathbf{x}(t)] + W[\mathbf{x}(t)] - \Delta F\}} \\ &= \rho_B(\tilde{\mathbf{x}}(0)) e^{-\beta \tilde{S}[\tilde{\mathbf{x}}(t)]}, \end{aligned} \quad (13)$$

where  $\rho_B(\mathbf{x}) = e^{-\beta[U_B(\mathbf{x}) - F_B]}$  is the equilibrium distribution for  $U_B(\mathbf{x})$ , and

$$\tilde{S}[\tilde{\mathbf{x}}(t)] = (\text{I}) \int_0^{t_f} \frac{|\dot{\tilde{\mathbf{x}}} + \nabla(\tilde{U}_0 - \tilde{U}_1)|^2}{4} dt \quad (14)$$

has the form of a path action, with  $\tilde{U}_{0,1}(\mathbf{x}, t) = U_{0,1}(\mathbf{x}, t_f - t)$  denoting the time-reversed potential energies. Eq. (13) gives the probability of observing the path  $\tilde{\mathbf{x}}(t)$  under the Langevin equation

$$\dot{\tilde{\mathbf{x}}} = -\nabla(\tilde{U}_0 - \tilde{U}_1) + \boldsymbol{\eta}(t) \quad \text{with} \quad \tilde{\mathbf{x}}(0) \sim \rho_B(\cdot), \quad (15)$$

differing from Eq. (6) by a minus sign on the  $U_1$  term. In other words, the reverse path ensemble that satisfies Eq. (13) for the time-asymmetric work Eq. (7) is one that is driven by a protocol  $\tilde{U}_0 - \tilde{U}_1$  that is *different* from the time-reversal of the forward protocol  $U_0 + U_1$ . One can also verify that its associated definition of work

$$\tilde{W}[\tilde{\mathbf{x}}(t)] = \int_0^{t_f} \frac{\partial \tilde{U}_0}{\partial t} - \nabla \tilde{U}_0 \cdot \nabla(-\tilde{U}_1) + \beta^{-1} \nabla^2(-\tilde{U}_1) dt, \quad (16)$$

satisfies  $\tilde{W}[\tilde{\mathbf{x}}(t)] = -W[\mathbf{x}(t)]$ , so the same optimal  $U_0(\mathbf{x}, t)$  and  $U_1(\mathbf{x}, t)$  satisfying Eq. (8) also give  $\tilde{W}[\tilde{\mathbf{x}}(t)] = -\Delta F$  for every trajectory.

Through standard methods [18], the fluctuation theorem Eq. (3) follows directly from the microscopic fluctuation theorem Eq. (13). Thus, the time-asymmetric work (Eq. (7)) holds a deeper significance than how it may first appear – it relates the forward and reverse path ensembles given by Eqs. (6) and (15) that are driven by time-asymmetric protocols. We now exploit this to efficiently calculate free energy differences.

*Algorithm.*—In this section we present an on-the-fly adaptive importance-sampling protocol optimization algorithm, inspired by [19], that uses the previously collected bi-directional samples to iteratively discover lower-variance time-asymmetric protocols. Exploiting the mathematical structure of the Onsager-Machlup action, our algorithm requires minimal computational overhead, solely the inclusion of easily-computable auxiliary variables in each trajectory’s time-evolution.

Concretely, we consider the objective function

$$J = J_F + J_R = \langle W \rangle_F + \langle \tilde{W} \rangle_R. \quad (17)$$

Jensen’s inequality applied to Eq. (2) implies  $\langle W \rangle_F \geq \Delta F$  and  $\langle \tilde{W} \rangle_R \geq -\Delta F$ , with equality only for zero-variance optimal protocols.

Our simulations are performed using the Euler-Mayurama method to discretize Eqs. (6) and (15). The authors of [20] showed that instead of discretizing the work functional (in our case Eq. (7)), by using the expression derived from Eq. (13)

$$W[\mathbf{x}(t)] = U_B(x(t_f)) - U_A(\mathbf{x}(0)) + \beta^{-1} \ln \frac{P[\mathbf{x}(t)|\mathbf{x}(0)]}{\tilde{P}[\tilde{\mathbf{x}}(t)|\tilde{\mathbf{x}}(0)]}$$

with the correct discrete-path probabilities, time-discretization-induced errors can be fully eliminated. In our setting this may be written as

$$W[\mathbf{x}(t)] = \{U_B(x(t_f)) + \tilde{S}[\tilde{\mathbf{x}}(t)]\} - \{U_A(\mathbf{x}(0)) + S[\mathbf{x}(t)]\} \quad (18)$$

and is what we measure for each trajectory.

From now on we will use Einstein notation, where repeated upper and lower Greek indices signify summation. Let  $\{U_\mu(\mathbf{x}, t) | \mu = 1, \dots, M\}$  denote a set of time-dependent basis functions. Given the linear parameterization of the forward and reverse protocols  $U_F = U_0 + U_1$  and  $U_R = U_0 - U_1$

$$U_{F,R}(\mathbf{x}, t) = \begin{cases} U_A(\mathbf{x}) & \text{for } t = 0 \\ \theta_{F,R}^\mu U_\mu(\mathbf{x}, t) & \text{for } t \in (0, t_f) \\ U_B(\mathbf{x}) & \text{for } t = t_f \end{cases} \quad (19)$$

with parameters  $\theta = (\theta_F, \theta_R) \in \mathbb{R}^{2M}$ , the Onsager-Machlup path action Eq. (12) and the time-asymmetric work Eq. (18) become quadratic in  $\theta$

$$S[\mathbf{x}(t); \theta] = \theta_F^\mu \theta_F^\nu \mathbf{a}_{\mu\nu} + \theta_F^\mu \mathbf{b}_\mu + \theta\text{-ind. terms} \quad (20)$$

$$W[\mathbf{x}(t); \theta] = -(\theta_F^\mu \theta_F^\nu \mathbf{a}_{\mu\nu} + \theta_F^\mu \mathbf{b}_\mu + \mathbf{c}) + (\theta_R^\mu \theta_R^\nu \tilde{\mathbf{a}}_{\mu\nu} + \theta_R^\mu \tilde{\mathbf{b}}_\mu + \tilde{\mathbf{c}}), \quad (21)$$

where

$$\begin{aligned} \mathbf{a}_{\mu\nu} &= (\mathbf{I}) \int_0^{t_f} \frac{\nabla U_\mu \cdot \nabla U_\nu}{4} dt, & \tilde{\mathbf{a}}_{\mu\nu} &= (\mathbf{BI}) \int_0^{t_f} \frac{\nabla U_\mu \cdot \nabla U_\nu}{4} dt, \\ \mathbf{b}_\mu &= (\mathbf{I}) \int_0^{t_f} \frac{\dot{\mathbf{x}} \cdot \nabla U_\mu}{2} dt, & \tilde{\mathbf{b}}_\mu &= -(\mathbf{BI}) \int_0^{t_f} \frac{\dot{\mathbf{x}} \cdot \nabla U_\mu}{2} dt, \\ \mathbf{c} &= U_A(\mathbf{x}(0)), & \text{and } \tilde{\mathbf{c}} &= U_B(x(t_f)) \end{aligned} \quad (22)$$

are  $\theta$ -independent functionals of the time-discretized trajectory  $\mathbf{x}(t)$  [21]. Here, (BI) refers to a Backwards Itô integral, needed to write terms of the reverse ensemble  $\tilde{S}[\tilde{\mathbf{x}}(t)]$  as a functional of  $\mathbf{x}(t)$ . (Eqs. (20)–(22) apply for the reverse path ensemble  $\tilde{S}[\tilde{\mathbf{x}}(t)], \tilde{W}[\tilde{\mathbf{x}}(t)]$ , through the transformation  $t \rightarrow t_f - t$ ,  $\{F, R\} \rightarrow \{R, F\}$ .) These variables  $\mathbf{a}, \tilde{\mathbf{a}} \in \mathbb{R}^{M \times M}$ ,  $\mathbf{b}, \tilde{\mathbf{b}} \in \mathbb{R}^M$ , and  $\mathbf{c}, \tilde{\mathbf{c}} \in \mathbb{R}$  are akin to the eligibility trace variables (sometimes called “malliavin weights”) used in reinforcement learning policy-gradient algorithms [22–26], which are dynamically evolved with each trajectory  $\mathbf{x}(t)$ .

In the following two paragraphs we consider only the forward ensemble for simplicity. If for every trajectory  $\mathbf{x}^i(t)$ , as well as the work  $W^i$  we calculate its functional values  $(\mathbf{a}^i, \mathbf{b}^i, \mathbf{c}^i, \tilde{\mathbf{a}}^i, \tilde{\mathbf{b}}^i, \tilde{\mathbf{c}}^i)$  and keep track of the  $\theta^i = (\theta_F^i, \theta_R^i)$  under which it was produced, then the  $\theta$ -dependent importance-sampling estimator may be constructed

$$\hat{J}_F(\theta) = \frac{\sum_{i=1}^{n_s} \mathbf{r}_F^i(\theta) \mathbf{w}_F^i(\theta)}{\sum_{i=1}^{n_s} \mathbf{r}_F^i(\theta)}, \quad (23)$$

where the sum is over collected forward samples  $i$ ,  $\mathbf{r}_F^i(\theta)$  is the likelihood ratio (i.e., the Radon–Nikodym derivative)

$$\mathbf{r}_F^i(\theta) = \frac{P[\mathbf{x}^i(t) \text{ from } \theta]}{P[\mathbf{x}^i(t) \text{ from } \theta^i]} = e^{-\beta(S[\mathbf{x}^i(t); \theta] - S[\mathbf{x}^i(t); \theta^i])}, \quad (24)$$

and  $\mathbf{w}^i(\theta) = W[\mathbf{x}^i(t); \theta]$  is the time-asymmetric work for the trajectory  $\mathbf{x}^i(t)$  as if it were sampled under  $\theta$  instead of  $\theta^i$ . The protocol may be optimized by minimizing Eq. (23).

Of course, the quality of the importance-sampling estimate Eq. (23) degrades the further away the input  $\theta$  is from the set of  $\theta^i$  under which samples were collected. One common heuristic of this degradation is the effective sample size [27]

$$n_F^{\text{eff}}(\theta) = \frac{\left( \sum_{i=1}^{n_s} \mathbf{r}_F^i(\theta) \right)^2}{\sum_{i=1}^{n_s} \mathbf{r}_F^i(\theta)^2}, \quad (25)$$

ranging from 1 (uneven  $\mathbf{r}_F^i$  values, high degradation) to  $n_s$  (equal  $\mathbf{r}_F^i$  values, low degradation).

We now state our algorithm (pseudocode given in Alg. 1): at each iteration, an equal number of independent forward and reverse trajectories are simulated through Eqs. (6) and (15) using the  $U_F, U_R$  specified by current parameters  $\theta_{\text{curr}}$ , with the time-asymmetric work

$W$  and auxiliary variables  $(\mathbf{a}, \mathbf{b}, \mathbf{c}, \tilde{\mathbf{a}}, \tilde{\mathbf{b}}, \tilde{\mathbf{c}})$  of each trajectory dynamically calculated; then the protocol is updated through solving the nonlinear constrained optimization problem

$$\theta_{\text{next}} = \text{argmin}_{\theta} \{ \hat{J}(\theta) \mid \{n_F^{\text{eff}}(\theta), n_R^{\text{eff}}(\theta)\} \geq f n_s \}, \quad (26)$$

for which there are efficient numerical solvers (e.g. SLSQP [28] pre-implemented in SciPy [29]). Here  $\hat{J}(\theta) = \hat{J}_F(\theta) + \hat{J}_R(\theta)$ ,  $n_F^{\text{eff}}(\theta)$  and  $n_R^{\text{eff}}(\theta)$  are constructed with the  $n_s$  forward and  $n_s$  reverse samples collected over all iterations, and  $f \in [0, 1]$  is a hyperparameter specifying the constraint strength: the fraction of total samples we are constraining  $n_{F,R}^{\text{eff}}$  to be greater or equal than. Finally,  $\widehat{\Delta F}_{\text{BAR}}$  is calculated with the bi-directional work measurements collected across all iterations using Eq. (4), which is permitted by the satisfaction of Eq. (5).

*Basis set.*—We chose our basis set in order to represent protocols of the form

$$U(\mathbf{x}, t) = \lambda_A(t) U_A(\mathbf{x}) + \lambda_B(t) U_B(\mathbf{x}) + \lambda_C(t) U_C(\mathbf{x}) \quad (27)$$

where  $U_C(\mathbf{x})$  is a linear quasi-counterdiabatic potential

$$U_C(\mathbf{x}) = -\mathbf{c} \cdot \mathbf{x} \quad \text{with} \quad \mathbf{c} = \frac{\langle \mathbf{x} \rangle_B - \langle \mathbf{x} \rangle_A}{t_f} \quad (28)$$

directly forcing each coordinate  $x_n$  with magnitude proportional to the difference of its equilibrium values  $\langle \mathbf{x} \rangle_{A,B} = \int \mathbf{x} \rho_{A,B}(\mathbf{x}) d\mathbf{x}$  [30]. The basis set is

$$\left\{ U_{\ell}(\mathbf{x}) p_m \left( \frac{2t}{t_f} - 1 \right) \mid \ell \in \{A, B, C\}, 0 \leq m \leq m_{\max} \right\}, \quad (29)$$

where  $p_m(\cdot)$  is the  $m$ -th Legendre polynomial.

For all numerical examples,  $m_{\max} = 4$  was used and the algorithm was initialized with 120 bi-directional samples drawn from a naive protocol  $\lambda_A(t) = 1 - t/t_f$ ,  $\lambda_B(t) = t/t_f$ ,  $\lambda_C(t) = 0$ . At each iteration Eq. (26) was solved for  $n_{\text{mb}} = 20$  independently subsampled mini-batches of size  $n_s^{\text{mb}} = 80$  with  $f = 0.3$ ; the protocol was then updated to the minibatch-averaged  $\theta_{\text{next}}$ ; finally, 20 additional bi-directional samples were drawn with the new protocol. In total, 44 iterations were performed, giving 1000 bi-directional samples. [18]

*Linearly-Biased double well.*—The first system we consider is a one-dimensional quartic double-well with a linear bias (Fig. 1(a)). The potentials are  $U_A(x) = E_0[(x^2 - 1)^2/4 - x]$ ,  $U_B(x) = E_0[(x^2 - 1)^2/4 + x]$  (cf. [31] for optimal protocols minimizing  $\langle W_{\text{trad}} \rangle_F$ ). We set  $U_C(x) = 0$  because  $U_B(x) - U_A(x)$  is already linear in  $x$ . We use  $\beta = 1$ ,  $E_0 = 16$ , and a timestep  $\Delta t = 1 \times 10^{-3}\tau$  where  $\tau = 1$  is the natural timescale (we have length scale  $\ell = \beta = \gamma = 1$ ).

Fig. 1(b) displays the  $\widehat{\Delta F}_{\text{BAR}}$  estimator mean squared error for 1000 bi-directional work measurements collected

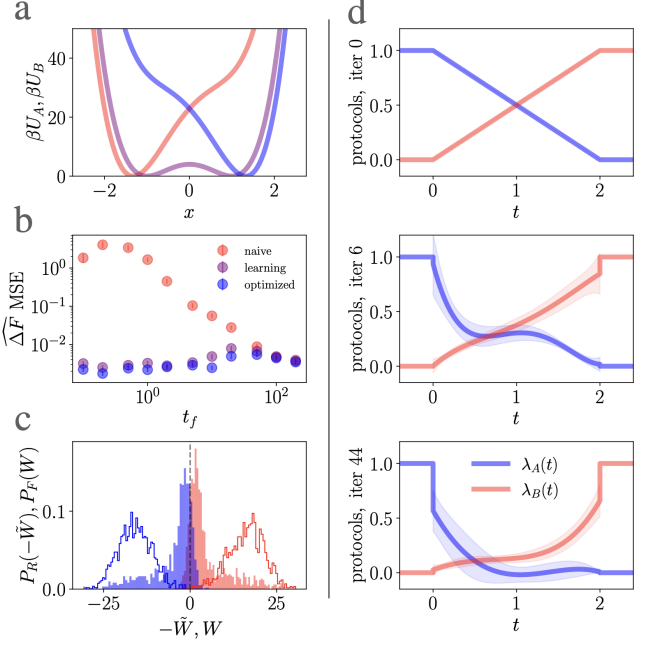


FIG. 1. (a) The potentials  $U_A(x)$  (red) and  $U_B(x)$  (blue) are obtained by linearly biasing a double well (purple). (b)  $\widehat{\Delta F}_{\text{BAR}}$  mean squared error from 1000 bi-directional measurements drawn solely from the naive protocol (red), cumulatively from protocols that are adaptively optimized (“learning”) with our algorithm (purple), and solely from the last-iteration (“optimized”) protocols (blue) for various protocol times  $t_f$ . (c) Single-trial  $P_F(W)$  (red) and  $P_R(-W)$  (blue) work distributions for 1000 measurements from the naive protocol, (unfilled) and adaptively optimized protocols (shaded) for  $t_f = 2$ , the ground truth shown as a grey dashed line. Measurements made with protocol optimization have significantly more overlap, leading to lower estimator error. (d) Forward protocols  $\lambda_A(t)$  (blue) and  $\lambda_B(t)$  (red) at various iterations of protocol optimization for  $t_f = 2$ . Shaded region represents variability across 100 independent trials. In the optimized last-iteration protocol,  $\lambda_A(t) + \lambda_B(t)$  (giving the energy scale) is greatly reduced at intermediate times, while  $\lambda_B(t) - \lambda_A(t)$  (giving the linear bias) is time-asymmetrically shifted. The reverse protocols (not shown here) are similar [18].

solely from the naive protocol (red), the 1000 measurements collected cumulatively over on-the-fly protocol optimization (purple), and 1000 measurements collected solely from the last-iteration (blue). Each dot represents the empirical average over 100 independent trials. Note that the mean squared error is up to 1600 times lower under protocol optimization compared to under the naive protocol (obtained at  $t_f = 0.2$ ). For  $t_f \gtrsim 10$  the algorithm does not converge within the 1000 measurements [18], leading to less improvement. Fig. 1(c) shows that bi-directional work measurements collected under the protocol optimization algorithm have significantly more overlap than measurements collected from the naive protocol,

leading to reduced estimator error. Fig. 1(d) gives snapshots on how the optimal protocol is adaptively learned.

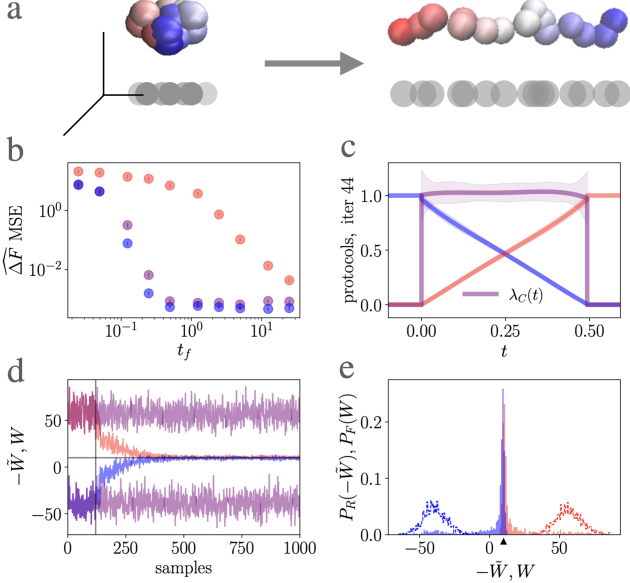


FIG. 2. (a) A Rouse polymer is stretched from a collapsed state to an extended one. (b)  $\bar{\Delta F}_{\text{BAR}}$  mean squared error versus protocol time, points colored as in Fig. 1. (c) For moderate protocol times ( $t_f = 0.5 \tau_R$  displayed here) the optimized protocol ( $\lambda_A(t), \lambda_B(t), \lambda_C(t)$ ) learned in 44 iterations is the counterdiabatic protocol Eq. (30). (d) Single-trial bi-directional work samples from the naive protocol ( $W$  and  $-\tilde{W}$  purple) and adaptively-optimized protocols ( $W$  red,  $-\tilde{W}$  blue) for  $t_f = 0.5 \tau_R$ . Vertical line demarcates start of protocol optimization. The ground truth  $\Delta F$  is shown as a horizontal line. (e) Work distributions corresponding to the samples in (d). The ground truth is indicated by the triangular arrow. Cumulative measurements made under protocol optimization (shaded) have dramatically greater overlap than measurements made under the naive protocols (unfilled), leading to lower estimator error.

*Rouse polymer*— Next we consider a  $(N + 1)$ -bead Rouse polymer (Fig. 2(a)) with stiffness  $k$  and intrinsic energy given by  $U_{\text{Rouse}}(x_0, x_1, \dots, x_N) = \sum_{n=0}^{N-1} (k/2)(x_{n+1} - x_n)^2$  from harmonic bonds between adjacent beads [32, 33]. We estimate  $\Delta F$  between a collapsed state (fixing  $x_0 = x_N = 0$ ) and an extended state (fixing  $x_0 = 0, x_N = \lambda_f$ ), so our configuration space is  $\mathbf{x} \in \mathbb{R}^{N-1}$  with potential energies  $U_A(x_1, \dots, x_{N-1}) = U_{\text{Rouse}}(0, x_1, \dots, x_{N-1}, 0)$  and  $U_B(x_1, \dots, x_{N-1}) = U_{\text{Rouse}}(0, x_1, \dots, x_{N-1}, \lambda_f)$ . Equilibrium averages  $\langle x_n \rangle_A = 0, \langle x_n \rangle_B = n\lambda_f/N$  give  $U_C(\mathbf{x}) = -(\lambda_f/Nt_f) \sum_{n=1}^N nx_n$ , and the ground truth is  $\Delta F = F_B - F_A = k\lambda_f^2/(2N)$ . It may be verified that for this problem the time-varying potential energies

$$U_0(\mathbf{x}, t) = \left(1 - \frac{t}{t_f}\right)U_A(\mathbf{x}) + \left(\frac{t}{t_f}\right)U_B(\mathbf{x})$$

$$U_1(\mathbf{x}, t) = U_C(\mathbf{x}) \quad (30)$$

solve Eq. (9) and are thus counterdiabatic.

We use  $\beta = k = 1$ ,  $N = 20$ , and timestep  $\Delta t = 2.5 \times 10^{-5} \tau_R$  where  $\tau_R = \beta N^2/\pi^2$  is the Rouse relaxation time [32]. Initial conditions for  $\rho_A(\mathbf{x})$  and  $\rho_B(\mathbf{x})$  were drawn from a normal-modes basis [18]. Fig. 2(b) shows an improvement of up to 8300 (for  $t_f = 0.5\tau_R$ ) in  $\bar{\Delta F}_{\text{BAR}}$  mean squared error between naive and optimized protocols. The counterdiabatic solution Eq. (30) corresponds to  $\lambda_A(t) = (1 - t/t_f), \lambda_B(t) = t/t_f$ , and  $\lambda_C(t) = 1$ , which what the algorithm learns for  $t_f = \tau_R$  as depicted in Fig. 2(c). (This was generally the case for  $t_f \geq 0.5\tau_R$ . For  $t_f < 0.5\tau_R$  the algorithm learns a sub-optimal local solution that still provides some improvement [18].) Fig. 2(d) shows single-trial traces of bi-directional work measurements for the naive protocol (purple) and adaptively-optimized protocols (red for  $W$ , blue for  $-\tilde{W}$ ) for  $t_f = 0.5\tau_R$ . The protocol converges in  $\sim 500$  samples /  $\sim 20$  iterations, and then consistently gives work measurements closely centered at the ground truth free energy (gray horizontal line). Histograms of these traces (filled) are shown in Fig. 2(e), exhibiting a remarkable increase in the overlap compared with their naive counterparts (lines).

*Worm-like chain with attractive linker*— We now consider a  $(N + 1)$ -bead worm-like chain model (WLC) in 2 dimensions with an added Lennard-Jones interaction between the first and last beads (similar to the 3rd example of [34]). Fixing  $(x_0, y_0) = (0, 0)$ , the configuration space is  $\vec{\phi} \in \mathbb{R}^N$ , where  $\phi_n$  is the angle of the  $n$ th bond with respect to the  $x$ -axis, with  $(x_n(\vec{\phi}), y_n(\vec{\phi})) = (\sum_{m=1}^n \cos \phi_m, \sum_{m=1}^n \sin \phi_m)$ . The angular potential  $U_\phi = k \sum_{n=1}^{N-1} [1 - \cos(\phi_{n+1} - \phi_n)]$  penalizes the bending of adjacent bonds, and  $U_{\text{LJ}} = 4\epsilon_{\text{LJ}}[(\sigma_{\text{LJ}}/R)^{12} - (\sigma_{\text{LJ}}/R)^6]$  specifies the interaction between first and last beads, where  $R = \sqrt{x_N^2 + y_N^2}$  is the end-to-end distance. We take  $k = 6, \beta = 1, \epsilon_{\text{LJ}} = 8, \sigma_{\text{LJ}} = 4$ , and  $N = 15$ .

Fig. 3(a) displays the conditioned free energy  $F(X/N) := -\beta^{-1} \ln \rho_{\text{eq}}(x_N = X, y_N = 0)$ , where  $\rho_{\text{eq}}$  is the equilibrium probability of observing some  $(x_N, y_N)$  under  $U = U_\phi + U_{\text{LJ}}$  [35] (constructed from  $10^7$  equilibrium samples of  $U_\phi$ , obtained with the Metropolis-adjusted Langevin Algorithm, that were reweighted by  $U_{\text{LJ}}$ ).  $F(X/N)$  exhibits a deep well for  $X_A \approx 2^{1/6} \sigma_{\text{LJ}}$  (trapped/bent state) and a shallow well at large  $X_B \approx 0.9N$  (free/relaxed state), separated by a barrier; their difference in value  $\Delta F \approx 5.3$  may be calculated by estimating the  $\Delta F$  between  $U_A(\vec{\phi}) = U_\phi + U_{\text{LJ}} + (k_{\text{ext}}/2)[(x_N - \lambda_i)^2 + y_N^2]$  and  $U_B(\vec{\phi}) = U_\phi + U_{\text{LJ}} + (k_{\text{ext}}/2)[(x_N - \lambda_f)^2 + y_N^2]$  for  $\lambda_i = 2^{1/6} \sigma_{\text{LJ}}, \lambda_f = 0.9N$ , and  $k_{\text{ext}} \gg 1$ .

We calculate the  $\Delta F$  between  $U_A$  and  $U_B$  for  $k_{\text{ext}} = 200$ . We use timestep  $\Delta t = 1.41 \times 10^{-4} \tau_{\text{LJ}}$  where  $\tau_{\text{LJ}} = \sqrt{\epsilon_{\text{LJ}}/\sigma^2}$  is the Lennard-Jones timescale.  $U_C(\phi)$  is constructed with  $\langle x_n \rangle_B - \langle x_n \rangle_A$  and  $\langle y_n \rangle_B - \langle y_n \rangle_A$  from equilibrium samples of  $\rho_A$  and  $\rho_B$ . Fig. 3(b) displays single-trial work histograms for  $t_f = 0.28 \tau_{\text{LJ}}$ , showing work measurements much closer to the ground truth with protocol optimization, compared to the naive protocol. Fig. 3(c) shows the updating  $\widehat{\Delta F}_{\text{BAR}}$  estimator over 100 independent trials converges much more rapidly to the ground truth. With all 1000 bi-directional samples the mean squared error is 120 times lower with protocol optimization than with the naive protocol.

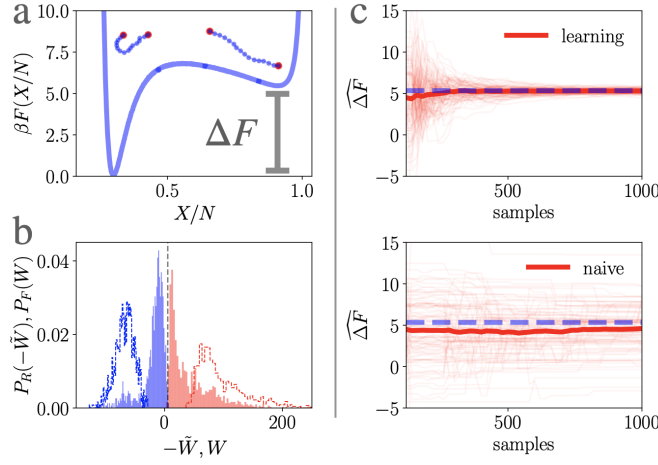


FIG. 3. Worm-like chain with an attractive linker. (a) Ground truth free energy surface relative to its value at  $X_A = 2^{1/6} \sigma_{\text{LJ}}$ ; the left well corresponds to the ends of the chain bound to one another and the right well corresponds to a nearly straight configuration. (b) Work distributions before (unfilled) and during (filled) optimization for  $t_f = 0.28$ , the ground truth shown as a grey dashed line. (c) The  $\widehat{\Delta F}_{\text{BAR}}$  estimator updated over the 1000 samples converges to the ground truth value much more quickly under protocol optimization than under the naive protocol.

*Discussion.*—In this Letter we have demonstrated the microscopic fluctuation theorem for the time-asymmetric work and proposed an on-the-fly time-asymmetric protocol optimization algorithm whose effectiveness we illustrated with three toy models of varying complexity. Time-asymmetric protocols have been considered before [36–38], but to our knowledge we are the first to use  $\widehat{\Delta F}_{\text{BAR}}$  on bi-directional work measurements from adaptive time-asymmetric protocols. A clear next step is to test our algorithm on more physically realistic systems. This work should be straightforward to implement with JAX-MD [39]. In principle our algorithm should work with underdamped dynamics [37], and it should also be possible to adaptively optimize the protocol time  $t_f$  and sampling ratio  $n_F/n_R$ .

Our method exploits the quadratic structure of the

Onsager-Machlup path action to construct  $\hat{J}(\theta)$ , allowing for fast convergence given limited samples by using all samples in each optimization step. Typically the most computationally expensive step in a molecular dynamics simulation is calculating potential energy gradients  $\nabla U$  to evolve  $\mathbf{x}(t)$ , which does not need to be repeated to evolve  $(\mathbf{a}_{\mu\nu}, \mathbf{b}_\mu, \dots)$ . A valid critique of our algorithm is that the number of auxiliary variables included with each trajectory scales quadratically with the number of basis functions, becoming prohibitively large when considering, for example, a separate control force on each particle of a many particle system. However, we have shown that a small number of basis functions to represent Eq. (27) already produces a substantial improvement in efficiency for our three examples. That said, it is straightforward to add additional basis functions (cf. Eq. (2) of [40]), which may be useful for more complex and realistic systems. It would be interesting to apply recent methods [41] to learn the optimal set of additional basis functions, that apply force along specific coordinates: bonds, angles, native contacts and other collective variables to further improve performance for larger scale systems.

The authors would like to thank Nilesh Tripuraneni, Hunter Akins, Chris Jarzynski, and Gavin Crooks for useful discussions, and Evie Pai for lending personal computing resources. This research used the Savio computational cluster resource provided by the Berkeley Research Computing program at the University of California, Berkeley (supported by the University of California Berkeley Chancellor, Vice Chancellor for Research, and Chief Information Officer). AZ is supported by the Department of Defense (DoD) through the National Defense Science & Engineering Graduate (NDSEG) Fellowship Program. BKS is supported by the Kavli Energy Nanoscience institute through the Philomathia Foundation Fellowship. This work was supported in part by the U.S. Army Research Laboratory and the U.S. Army Research Office under contract W911NF-20-1-0151.

Documented code for this project is currently in preparation.

\* adrzhong@berkeley.edu, biophysben@gmail.com.  
These authors contributed equally.

- [1] S. Ejiri, Y. Maezawa, N. Ukita, S. Aoki, T. Hatsuda, N. Ishii, K. Kanaya, T. Umeda, W.-Q. Collaboration, *et al.*, *Physical review D* **82**, 014508 (2010).
- [2] G. Tawa, I. Topol, S. Burt, R. Caldwell, and A. Rashin, *The Journal of Chemical Physics* **109**, 4852 (1998).
- [3] C. P. Kelly, C. J. Cramer, and D. G. Truhlar, *The Journal of Physical Chemistry B* **110**, 16066 (2006).
- [4] C. Chipot and A. Pohorille, *Free energy calculations*, Vol. 86 (Springer, 2007).
- [5] M. R. Shirts, D. L. Mobley, and S. P. Brown, *Drug Design* **1**, 61 (2010).
- [6] Z. Cournia, C. Chipot, B. Roux, D. M. York, and

W. Sherman, in *Free Energy Methods in Drug Discovery: Current State and Future Directions* (ACS Publications, 2021) pp. 1–38.

[7] M. R. Shirts and V. S. Pande, *The Journal of chemical physics* **122**, 144107 (2005).

[8] M. R. Shirts, E. Bair, G. Hooker, and V. S. Pande, *Physical review letters* **91**, 140601 (2003).

[9] C. H. Bennett, *Journal of Computational Physics* **22**, 245 (1976).

[10] G. E. Crooks, *Journal of Statistical Physics* **90**, 1481 (1998).

[11] G. E. Crooks, *Physical Review E* **60**, 2721 (1999).

[12] S. Vaikuntanathan and C. Jarzynski, *Physical Review Letters* **100**, 190601 (2008).

[13] Typically there is a factor of the friction coefficient  $\gamma$  multiplying the left side of Eq. (6). For notational simplicity we have set it to one, which may always be done through a time-rescaling.

[14] E. Ilker, Ö. Güngör, B. Kuznets-Speck, J. Chiel, S. Deffner, and M. Hinczewski, *Physical Review X* **12**, 021048 (2022).

[15] S. Iram, E. Dolson, J. Chiel, J. Pelesko, N. Krishnan, Ö. Güngör, B. Kuznets-Speck, S. Deffner, E. Ilker, J. G. Scott, *et al.*, *Nature Physics* **17**, 135 (2021).

[16] A. G. Frim, A. Zhong, S.-F. Chen, D. Mandal, and M. R. DeWeese, *Physical Review E* **103**, L030102 (2021).

[17] A. B. Adib, *The Journal of Physical Chemistry B* **112**, 5910 (2008).

[18] Supplementary material currently in preparation.

[19] T. Jie and P. Abbeel, *Advances in Neural Information Processing Systems* **23** (2010).

[20] D. A. Sivak, J. D. Chodera, and G. E. Crooks, *Physical Review X* **3**, 011007 (2013).

[21] The astute reader might point out that under the rules of stochastic calculus, how they are written out  $\mathbf{a} = \tilde{\mathbf{a}}$  for all  $\mathbf{x}(t)$ . However, they are different under a finite time-discretization, and must both be kept track of to eliminate time-discretization error.

[22] R. J. Williams, *Reinforcement learning* , 5 (1992).

[23] J. Peters and S. Schaal, *Neural networks* **21**, 682 (2008).

[24] P. B. Warren and R. J. Allen, *Physical review letters* **109**, 250601 (2012).

[25] A. Das and D. T. Limmer, *The Journal of chemical physics* **151**, 244123 (2019).

[26] A. Das, B. Kuznets-Speck, and D. T. Limmer, *Physical Review Letters* **128**, 028005 (2022).

[27] A. B. Owen, *Monte Carlo theory, methods and examples* (2013).

[28] D. Kraft, *Forschungsbericht- Deutsche Forschungs- und Versuchsanstalt fur Luft- und Raumfahrt* (1988).

[29] P. Virtanen, R. Gommers, T. E. Oliphant, M. Haberland, T. Reddy, D. Cournapeau, E. Burovski, P. Peterson, W. Weckesser, J. Bright, S. J. van der Walt, M. Brett, J. Wilson, K. J. Millman, N. Mayorov, A. R. J. Nelson, E. Jones, R. Kern, E. Larson, C. J. Carey, I. Polat, Y. Feng, E. W. Moore, J. VanderPlas, D. Laxalde, J. Perktold, R. Cimrman, I. Henriksen, E. A. Quintero, C. R. Harris, A. M. Archibald, A. H. Ribeiro, F. Pedregosa, P. van Mulbregt, and SciPy 1.0 Contributors, *Nature Methods* **17**, 261 (2020).

[30] The first two terms are a generalization of the protocol form  $U_\lambda(\mathbf{x}) = (1 - \lambda) U_A(\mathbf{x}) + \lambda U_B(\mathbf{x})$  commonly considered in stochastic thermodynamics. Typically, linear combinations of just  $U_A(\mathbf{x})$  and  $U_B(\mathbf{x})$  are not effective in transporting  $\rho_A(\mathbf{x}) \rightarrow \rho_B(\mathbf{x})$ , motivating our inclusion of the linear potential  $U_C(\mathbf{x})$ .

[31] A. Zhong and M. R. DeWeese, *Physical Review E* **106**, 044135 (2022).

[32] M. Doi, S. F. Edwards, and S. F. Edwards, *The theory of polymer dynamics*, Vol. 73 (oxford university press, 1988).

[33] Because of the harmonic nature of the interbead potential, the dynamics of the Rouse polymer separates in its 3 spatial dimensions; without loss of generality, we can consider just a single spatial dimension.

[34] B. Kuznets-Speck and D. T. Limmer, *Biophysical Journal* (2023), <https://doi.org/10.1016/j.bpj.2023.03.031>.

[35] From the change of coordinates  $R = \sqrt{x_N^2 + y_N^2}$ ,  $\vartheta = \tan^{-1}(y_N/x_N)$  and the radial symmetry of  $U_\phi$  and  $U_{\text{LJ}}$ , one has  $\rho_{\text{eq}}(R) \propto (2\pi R)^{-1} \rho_{\text{eq}}(x_N = R, y_N = 0)$ .

[36] G. Li, H. Quan, and Z. Tu, *Physical Review E* **96**, 012144 (2017).

[37] G. Li and Z. Tu, *Physical Review E* **100**, 012127 (2019).

[38] S. Blaber and D. A. Sivak, *The Journal of Chemical Physics* **153**, 244119 (2020).

[39] S. Schoenholz and E. D. Cubuk, *Advances in Neural Information Processing Systems* **33**, 11428 (2020).

[40] L. N. Naden, T. T. Pham, and M. R. Shirts, *Journal of Chemical Theory and Computation* **10**, 1128 (2014).

[41] A. N. Singh and D. T. Limmer, *arXiv preprint arXiv:2302.14857* (2023).

---

**Algorithm 1** Time-Asymmetric Protocol Optimization via Adaptive Importance Sampling

---

1: **inputs**  $\beta, U_A(\mathbf{x}), U_B(\mathbf{x})$ ; stepsize  $dt$ , number of timesteps  $N$ , basis functions  $\{U_\mu(\mathbf{x}, n) |_{n=1, \dots, N}\}$ , initial guess  $\theta_{\text{init}}$   
2: **parameters** Samples per iteration  $N_s$ , minibatches per iteration  $N_{\text{mb}}$ , minibatch size  $n_s^{\text{mb}}$ , constraint strength  $f$   
3: **given** Methods `DRAWSAMPLEA()`, `DRAWSAMPLEB()` that return equilibrium samples from  $\rho_A, \rho_B$   
4: **output** Iteratively updated  $\widehat{\Delta F}$  estimate  
5:  
6: **function** `RUNTRAJF`(parameters  $\theta = (\theta_F, \theta_R)$ ) ▷ Euler-Maruyama method  
7:   Obtain  $\mathbf{x}_0 \leftarrow \text{DRAWSAMPLEA}()$   
8:   Initialize  $\mathbf{x}, \mathbf{a}_{\mu\nu}, \mathbf{b}_\mu, \tilde{\mathbf{a}}_{\mu\nu}, \tilde{\mathbf{b}}_\mu \leftarrow \mathbf{x}_0, 0, 0, 0, 0$   
9:   **for**  $n = 1, \dots, N$  **do**  
10:     Evaluate  $\nabla U_\mu \leftarrow \nabla U_\mu(\mathbf{x}, n)$  for each  $\mu$   
11:     Calculate  $d\mathbf{x} \leftarrow -\theta_F^\mu \nabla U_\mu dt + \sqrt{2\beta^{-1}} dB$ , where  $dB \sim \mathcal{N}(0, dt \times I_d)$  is a  $d$ -dimensional normal random variable  
12:     Evaluate  $\nabla \tilde{U}_\mu \leftarrow \nabla U_\mu(\mathbf{x} + d\mathbf{x}, n)$  for each  $\mu$   
13:     Evolve  $\mathbf{x} \leftarrow \mathbf{x} + d\mathbf{x}$   
14:     Evolve  $\mathbf{a}_{\mu\nu}, \mathbf{b}_\mu \leftarrow \mathbf{a}_{\mu\nu} + \nabla U_\mu \cdot \nabla U_\nu dt/4, \mathbf{b}_\mu + \nabla U_\mu \cdot d\mathbf{x}/2$   
15:     Evolve  $\tilde{\mathbf{a}}_{\mu\nu}, \tilde{\mathbf{b}}_\mu \leftarrow \tilde{\mathbf{a}}_{\mu\nu} + \nabla \tilde{U}_\mu \cdot \nabla \tilde{U}_\nu dt/4, \tilde{\mathbf{b}}_\mu - \nabla \tilde{U}_\mu \cdot d\mathbf{x}/2$  ▷ This holds because  $d\tilde{\mathbf{x}} = -d\mathbf{x}$   
16:   **end for**  
17:   Evaluate  $\mathbf{c}, \tilde{\mathbf{c}} \leftarrow U_A(\mathbf{x}_0), U_B(\mathbf{x})$   
18:   Calculate  $W \leftarrow -(\theta_F^\mu \theta_F^\nu \mathbf{a}_{\mu\nu} + \theta_F^\mu \mathbf{b}_\mu + \mathbf{c}) + (\theta_R^\mu \theta_R^\nu \tilde{\mathbf{a}}_{\mu\nu} + \theta_R^\mu \tilde{\mathbf{b}}_\mu + \tilde{\mathbf{c}})$   
19:   **return**  $W, \mathbf{a}_{\mu\nu}, \mathbf{b}_\mu, \mathbf{c}, \tilde{\mathbf{a}}_{\mu\nu}, \tilde{\mathbf{b}}_\mu, \tilde{\mathbf{c}}, \theta$   
20: **end function**  
21:  
22: **function** `RUNTRAJR`(parameters  $\theta = (\theta_F, \theta_R)$ )  
23:   Obtain  $\tilde{\mathbf{x}}_0 \leftarrow \text{DRAWSAMPLEB}()$   
24:   Initialize  $\tilde{\mathbf{x}}, \tilde{\mathbf{a}}_{\mu\nu}, \tilde{\mathbf{b}}_\mu, \mathbf{a}_{\mu\nu}, \mathbf{b}_\mu \leftarrow \tilde{\mathbf{x}}_0, 0, 0, 0, 0$   
25:   **for**  $n = 1, \dots, N$  **do** ▷ because  $\nabla \tilde{U}_\mu(\cdot, n) = \nabla U_\mu(\cdot, N + 1 - n)$   
26:     Evaluate  $\nabla \tilde{U}_\mu \leftarrow \nabla U_\mu(\tilde{\mathbf{x}}, N + 1 - n)$  for each  $\mu$   
27:     Calculate  $d\tilde{\mathbf{x}} \leftarrow -\theta_R^\mu \nabla \tilde{U}_\mu dt + \sqrt{2\beta^{-1}} dB$ , where  $dB \sim \mathcal{N}(0, dt \times I_d)$  is a  $d$ -dimensional normal random variable  
28:     Evaluate  $\nabla U_\mu \leftarrow \nabla U_\mu(\tilde{\mathbf{x}} + d\tilde{\mathbf{x}}, N + 1 - n)$  for each  $\mu$   
29:     Evolve  $\tilde{\mathbf{x}} \leftarrow \tilde{\mathbf{x}} + d\tilde{\mathbf{x}}$   
30:     Evolve  $\tilde{\mathbf{a}}_{\mu\nu}, \tilde{\mathbf{b}}_\mu \leftarrow \tilde{\mathbf{a}}_{\mu\nu} + \nabla \tilde{U}_\mu \cdot \nabla \tilde{U}_\nu dt/4, \tilde{\mathbf{b}}_\mu + \nabla \tilde{U}_\mu \cdot d\tilde{\mathbf{x}}/2$   
31:     Evolve  $\mathbf{a}_{\mu\nu}, \mathbf{b}_\mu \leftarrow \mathbf{a}_{\mu\nu} + \nabla U_\mu \cdot \nabla U_\nu dt/4, \mathbf{b}_\mu - \nabla U_\mu \cdot d\tilde{\mathbf{x}}/2$   
32:   **end for**  
33:   Evaluate  $\tilde{\mathbf{c}}, \mathbf{c} \leftarrow U_B(\tilde{\mathbf{x}}_0), U_A(\tilde{\mathbf{x}})$   
34:   Calculate  $\tilde{W} \leftarrow -(\theta_R^\mu \theta_R^\nu \tilde{\mathbf{a}}_{\mu\nu} + \theta_R^\mu \tilde{\mathbf{b}}_\mu + \tilde{\mathbf{c}}) + (\theta_F^\mu \theta_F^\nu \mathbf{a}_{\mu\nu} + \theta_F^\mu \mathbf{b}_\mu + \mathbf{c})$   
35:   **return**  $\tilde{W}, \tilde{\mathbf{a}}_{\mu\nu}, \tilde{\mathbf{b}}_\mu, \tilde{\mathbf{c}}, \mathbf{a}_{\mu\nu}, \mathbf{b}_\mu, \mathbf{c}, \theta$   
36: **end function**  
37:  
38: **function** `UPDATETHETA`(forward samples  $\mathcal{S}_F$ , reverse samples  $\mathcal{S}_R$ )  
39:   Initialize  $\mathcal{S}_{\theta, \text{mb}} \leftarrow \{\}$   
40:   **repeat**  $N_{\text{mb}}$  **times** ▷ Use larger  $N_{\text{mb}}$  for larger  $|\mathcal{S}_F|$   
41:     Randomly select  $\mathcal{S}_F^{\text{mb}} \subset \mathcal{S}_F$  of size  $n_s^{\text{mb}}$  without replacement  
42:     Randomly select  $\mathcal{S}_R^{\text{mb}} \subset \mathcal{S}_R$  of size  $n_s^{\text{mb}}$  without replacement  
43:      $\theta^* \leftarrow \text{argmin}_\theta \{ \hat{J}_F(\theta; \mathcal{S}_F^{\text{mb}}) + \hat{J}_R(\theta; \mathcal{S}_R^{\text{mb}}) | n_F^{\text{eff}}(\theta; \mathcal{S}_F^{\text{mb}}) \geq f n_s^{\text{mb}}, n_R^{\text{eff}}(\theta; \mathcal{S}_R^{\text{mb}}) \geq f n_s^{\text{mb}} \}$   
44:      $\mathcal{S}_{\theta, \text{mb}}.\text{insert}(\theta^*)$   
45:   **end**  
46:   **return**  $\text{mean}(\mathcal{S}_{\theta, \text{mb}})$   
47: **end function**  
48:  
49: **procedure** `MAIN()`  
50:   Initialize parameters  $\theta \leftarrow \theta_{\text{init}}$  and sample arrays  $\mathcal{S}_F, \mathcal{S}_R \leftarrow \{\}, \{\}$   
51:   **repeat** ▷ Use  $N_{\text{mb}} + N_s$  on first iteration  
52:     **repeat**  $N_s$  **times**  
53:        $\mathcal{S}_F.\text{insert}(\text{RUNTRAJF}(\theta))$   
54:        $\mathcal{S}_R.\text{insert}(\text{RUNTRAJR}(\theta))$   
55:     **end**  
56:     Update estimate  $\widehat{\Delta F} \leftarrow \widehat{\Delta F}_{\text{BAR}}(\mathcal{S}_F, \mathcal{S}_R)$   
57:      $\theta \leftarrow \text{UPDATETHETA}(\mathcal{S}_F, \mathcal{S}_R)$   
58:   **until** out of computer time  
59: **end procedure**


---